

# Studies in a Random Noise Model of Decoherence

P. Korcyl, J. Wosiek

M. Smoluchowski Institute of Physics  
Jagellonian University, Reymonta 4, 30-059 Cracow, Poland

L. Stodolsky

Max-Planck-Institut für Physik (Werner-Heisenberg-Institut)  
Föhringer Ring 6, 80805 München, Germany

February 13, 2022

## Abstract

We study the effects of noise and decoherence for a double-potential well system, suitable for the fabrication of qubits and quantum logic elements. A random noise term is added to the hamiltonian, the resulting wavefunction found numerically and the density matrix obtained by averaging over noise signals. Analytic solutions using the two-state model are obtained and found to be generally in agreement with the numerical calculations.

In particular, a simple formula for the decoherence rate in terms of the noise parameters in the two-state model is reviewed and verified for the full simulation with the multi-level system. The formalism is extended to describe multiple sources of noise or different “dephasing” axes at the same time. Furthermore, the old formula for the “Turing-Watched Pot” effect is generalized to the case where the environmental interactions do not conserve the “quality” in question.

Various forms for the noise signal are investigated. An interesting result is the importance of the noise power at low frequency. If it vanishes there is, in leading order, no decoherence. This is verified in a numerical simulation where two apparently similar noise signals, but differing in the power at zero frequency, give strikingly different decoherence effects. A short discussion of situations dominated by low frequency noise is given.

## 1 Introduction

In the study of macroscopic quantum mechanics and quantum logic devices in particular, the question of decoherence and its effects remains an important, if not the most important, issue. Inevitable disturbances from the environment of the quantum device, and correlations established with variables of the environ-

ment, will limit the length of time for which the system under study acts as an isolated quantum system.

In previous work we studied, by means of numerical simulation, how decoherence affects and interacts with the behavior of some quantum logic devices [1]. The decoherence was modeled by a simple random noise signal presumed to act on a certain component of the system – in the SQUID corresponding to flux noise. In the present work we wish to consider more generally the connection between decoherence, the type of random noise signal, and the parts of the system upon which it acts. We reach a number of interesting conclusions on the effects of these factors.

A further interest of such studies is its connection with the “quantum measurement problem”, and we are able to illustrate quantitatively phenomena like the “Collapse of the Wavefunction” and the “Watched Pot Effect” through the simulations.

## 2 Hamiltonian

We shall examine the hamiltonian

$$H = \frac{-1}{2\mu} \frac{\partial^2}{\partial x^2} + V_0 \left\{ \frac{1}{2} [(x - x^{ext})^2] + \beta \cos x \right\} + H_{\mathcal{N}}(t), \quad (1)$$

which is suitable for representing a ”qubit” and through manipulations on  $x^{ext}$ , the quantum logic operations NOT and CNOT [1].

The first part of the expression represents a double potential well problem illustrated by Fig 1. The  $H_{\mathcal{N}}(t)$  represents a small, time dependent, random noise term. This will be used to simulate the decoherence effects. These could be due to either actual noise sources in the laboratory like stray fields, or true quantum mechanical decoherence due to unavoidable interactions of the simple idealized system with other variables.

The parameter  $x^{ext}$  controls the asymmetry of the two potential wells,  $x^{ext} = 0$  being the completely symmetric situation where the energy splitting between the two lowest levels  $\omega_{tunnel}$  is only due to the tunneling through the barrier. The height and width of the barrier are controlled by  $\beta$ . In the previous work it was found that the values  $\mu = V_o = 16.3$ ;  $\beta = 1.19$  give behavior suitable for quantum logic elements and we shall use these values in our simulations here. As seen on the figure, with these values there is a well defined pair of levels below the barrier. At the same time the barrier is low, giving a relatively large tunnel splitting. This permits the adiabatic sweeps, on which the gate operations are based, to be fast. For these values one has  $\omega_{tunnel} = 0.0044$ .

For the SQUID, these parameters are related to the inductance  $L$  and capacitance  $C$  by  $\mu = V_o \approx 1030 \sqrt{\frac{C/pF}{L/pH}}$ . The parameter  $\beta$  characterizes the critical current  $I_c$  and is given by  $\beta = \frac{2\pi L I_c}{\Phi_o}$ . (We use  $\hbar, c = 1$  units.) The overall energy scale is given by  $E_o = 1/\sqrt{LC}$  and the time unit by  $1/E_o = \sqrt{LC}$ . Thus the time unit is  $1.0 \times 10^{-12} \text{seconds} \times (L/pH C/pF)^{1/2}$ . With  $L = 400pH$  and

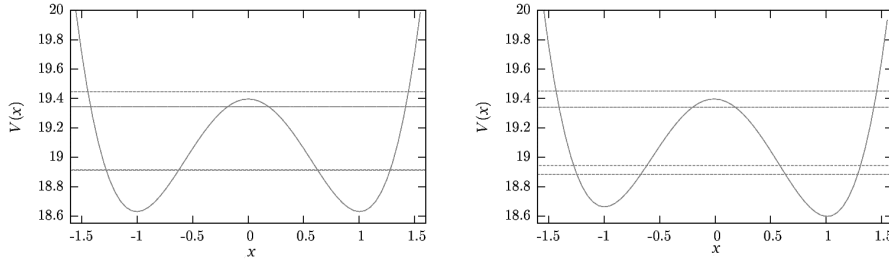


Figure 1: Double well potentials ( $V_o$  term) of the hamiltonian Eq 1, with the first four energy levels indicated. The left panel shows the symmetric configuration with  $x^{ext} = 0$  while the right one shows an asymmetric configuration with  $x^{ext} = 0.0020$ . The behavior of the two lowest levels is well represented by an effective hamiltonian  $H = \frac{1}{2}\sigma\mathbf{V}$ , where  $V_x$  is given by the tunneling energy and  $V_z$  by the asymmetry of the wells.

$C = 0.1pF$  for example,  $\omega_{tunnel} = 0.0044$  corresponds to  $\sim 4 \times 10^{-7}eV$ . The time unit is then  $6.3 \times 10^{-12} sec$ . [2].

The numerical methods are as outlined in [1], as introduced in [3]. A large basis of harmonic oscillator states is employed, and the resulting sparse hamiltonian matrix is inverted to find the energy eigenstates. The time evolution is found by repeated application of  $(1 + \frac{1}{2}iH\Delta t)/(1 - \frac{1}{2}iH\Delta t)$ .

### 3 Two-State System

The previous studies have shown that there is a range of parameter values where the two lowest levels for Eq 1 can be adequately represented as an effective two level system with hamiltonian  $H = \frac{1}{2}\sigma\mathbf{V}$ .

We use an (x,y,z) coordinate system for the various vectors in the following way.  $\mathbf{V}$  is approximately in the ‘z’ or ‘up’ direction when  $x^{ext}$  is relatively large so that the potential is asymmetric and the energy level splitting is essentially determined by the distance between the bottoms of the potential wells.  $\mathbf{V}$  is in the ‘x’ direction or ‘horizontal’ when  $x^{ext} = 0$  and the energy splitting is determined only by the tunneling through the barrier. Specifically, one determines [1] the components of  $\mathbf{V}$  to be  $V_z \approx 2V_o x^{ext} x_c$  and  $V_x = \omega_{tunnel}$ , the tunneling energy. The quantity  $x_c$  is the value of the x-coordinate where the wavefunction is centered when the wavefunction is localized in just one of the potential wells. For the parameter values used here this is always close to 1, about 0.9. The value of  $\omega_{tunnel}$ , namely =0.0044, is obtained from the numerical solutions as the level splitting for  $x^{ext} = 0$ , with the chosen parameters  $\mu = V_o = 16.3$ ;  $\beta = 1.19$ .

According to [1], deviations from the two-state model begin to appear when the level splitting for the lowest pair becomes comparable to the distance to the next set of levels. Various tests showed that the effective two-state description was good up to about  $x^{ext} \approx 0.01$ , where the level splitting was 0.30.

To represent the noise in this approximate two-state picture, we assume an additional term  $\frac{1}{2}\sigma\mathbf{B}$  in the two-state hamiltonian with a time dependent random field  $\mathbf{B}$ . The effective total two-state hamiltonian is then

$$H = \frac{1}{2}\sigma\mathbf{V} + \frac{1}{2}\sigma\mathbf{B}. \quad (2)$$

$\mathbf{B}$  thus represents a rapid small stochastic addition [5] to the  $\mathbf{V}$ . Just as for the components of  $\mathbf{V}$ , it is possible to establish relations between the  $\mathbf{B}$  and the parameters of  $H_{\mathcal{N}}$ . These will be given in section 7.

## 4 Density Matrix

Our object of study is the density matrix of the system. In our random noise model we generate it by inserting a particular realization  $\mathcal{N}^a(t)$  of a noise signal in the hamiltonian Eq 1 and then evolving an initial wavefunction to a final time with this hamiltonian  $H^a$ . Repeating the process, and averaging over many different noise realizations,  $N$ , gives a final density matrix:

$$\rho(t) = \overline{\psi\psi^\dagger} = \frac{1}{N} \sum_{a=1}^N \psi^a(t)\psi^{a\dagger}(t). \quad (3)$$

Although the evolution is unitary for a given  $\mathcal{N}^a(t)$ , the averaging process is not and the procedure evidently violates unitarity. The resulting density matrix will thus exhibit a time-dependent decoherence, which we wish to examine.

In particular we would like to study the decoherence for the effective two-level system comprised of the lowest states of the hamiltonian, with its  $2 \times 2$  density matrix. However, for the calculations with the full Eq 1, it must be noted that the resulting numerical density matrix Eq 3 is a function of two continuous variables in  $\rho(x', x)$ . Thus in principle Eq 3 refers not only to the two lowest states of the hamiltonian, but to the entire Hilbert space of the continuous  $x$  variable.

Nevertheless, in the previous studies it was found that in the region of parameter space where the two-state description is valid, the Hilbert space of lowest states is accurately spanned by one and the same set of wavefunctions even as the parameters of the hamiltonian are varied and the energy eigenstates change [4]. Therefore wavefunctions beginning in the two-state space remain there, and the results of evolving with Eq 1 can be expressed in the two-state space by projecting them onto the corresponding pair of wavefunctions. This is the procedure we will follow in the numerical evaluation of the  $2 \times 2$  density matrix.

On the other hand, for the simplified two-state or spin 1/2 system represented by Eq 2, the density matrix can be predicted analytically, as will be explained in section 5. This analytical result may be compared with that for the numerical procedure just described, where we insert the noise signal in Eq 1. To carry out this comparison one needs a translation between the noise signal

inserted in  $H_N$  and the equivalent  $\mathbf{B}$  in Eq2. This translation will be given in section 7.

The two-state density matrix can be parameterized in terms of Pauli matrices as

$$\rho = \frac{1}{2}(1 + \mathbf{P} \cdot \sigma) . \quad (4)$$

With our coordinate conventions  $\mathbf{P}$  is in the “up” or “down” or  $\pm z$  direction when the wavefunction is localized in one of the potential wells of Fig 1; and it is in the “horizontal” or  $\pm x$  direction when the wavefunction is the symmetric or antisymmetric combination of states in both potential wells.  $|\mathbf{P}| = P = 1$  corresponds to pure state and  $P < 1$  a mixed state.

In the two-state model the “polarization” vector  $\mathbf{P}$  evolves according to [14]

$$\dot{\mathbf{P}} = \mathbf{P} \times \mathbf{V} - D\mathbf{P}_T , \quad (5)$$

where the  $-D\mathbf{P}_T$  term represents the quantum damping or loss of coherence.  $D$  is the decoherence rate and  $D^{-1}$  is the decoherence time. This term reduces the components  $\mathbf{P}$  transverse to the direction chosen by the noise or decoherence interaction.

Although in the present paper we concentrate on situations with constant parameters in the hamiltonian (aside from the noise term), in previous work time dependent  $\mathbf{V}$  's were used. These may be employed to realize adiabatic quantum logic gates [1], and via the adiabatic method to give a direct measurement of  $D$  by a turning on-and-off of the classical-quantum transition [8].

## 5 D in the two-state model

We now consider how the decoherence or damping and the associated parameter  $D$  are generated by the random noise in the two-state picture of Eq2. The  $\mathbf{V}$  are assumed constant or slowly varying over the time period necessary to find the decoherence effects induced by the random fields. The method is essentially the same as in Ref [1] but we would like to present it in a somewhat more general form. This is nicely done by following Ref [9]. One considers the density matrix  $\rho = \frac{1}{2}(1 + \mathbf{P} \cdot \sigma)$  in the Heisenberg representation. The  $\mathbf{P}$  are also assumed to be slowly varying so that at a given time one may assume a certain initial density matrix which we call  $\rho(0)$ .

In Eq3 one may denote each of the terms on the right as  $\rho^a$ , so that  $\rho = \bar{\rho}^a$ . We then examine the density matrix equation  $\dot{\rho} = -i[H(t), \rho]$  term by term

$$\dot{\rho}^a = -i[H^a(t), \rho^a] , \quad (6)$$

iteratively:  $\rho(t) \approx \rho(0) + \rho_1 + \rho_2$ . The different orders refer to how many factors of the small  $\mathbf{B}$  occur and one compares equations with the same number of  $B$ 's [6]. Since we will assume the average value of the random fields  $\bar{\mathbf{B}}$  to be set to zero (or incorporated in the main hamiltonian), the first order contribution to the average  $\dot{\rho}$  is zero:  $\dot{\rho}_1 = -i[\bar{\sigma}\bar{\mathbf{B}}, \rho(0)] = 0$ . We thus consider the second order for  $\dot{\rho}$

$$\dot{\rho}_2^a(t) = -i\frac{1}{2}[\sigma\mathbf{B}^a, \rho_1^a] = -\frac{1}{4}[\sigma\mathbf{B}^a, [\sigma\mathbf{C}^a, \rho(0)]] \quad (7)$$

where we introduce the shorthand  $\mathbf{C}(t) = \int_0^t dt' \mathbf{B}(t')$  and use  $\rho_1 = -i\frac{1}{2}[\sigma\mathbf{C}, \rho(0)]$ .

Now in performing the average over the random fields in Eq 7, we will have to do with bilinear correlators between the vector components of  $B, C$ . These can be thought of as tensors of the type  $\overline{X_i Y_j}$ , where the average is over different realizations of the random fields. With just one random field in a fixed direction  $\mathbf{e}$ , one has

$$\overline{\mathbf{X} \otimes \mathbf{Y}} = \mathcal{C} \mathbf{e} \otimes \mathbf{e}^\dagger \quad (8)$$

for the tensor, where  $\mathcal{C}$  represents some quadratic correlator.

By making repeated use <sup>1</sup> of  $[\sigma\mathbf{X}, \sigma\mathbf{Y}] = i2\sigma\mathbf{X} \times \mathbf{Y}$  and comparing the resulting coefficients of  $\sigma$ , Eq 7 implies

$$\dot{\mathbf{P}} = \overline{BC}(\mathbf{e} \times (\mathbf{e} \times \mathbf{P})) . \quad (9)$$

To evaluate the correlator  $\overline{BC}$  we use the basic result from the theory of stationary random noise that the quantity  $(\int_0^t B(t') dt')^2 = 2t\mathcal{A}$ , where  $\mathcal{A}$  is the time integral of the autocorrelation function

$$\mathcal{A} = \int_0^\infty \overline{B(0)B(t)} dt . \quad (10)$$

Then

$$\overline{BC} = \overline{B(t) \int_0^t B(t') dt'} = \frac{1}{2} \frac{d}{dt} \left( \int_0^t B(t') dt' \right)^2 = \mathcal{A} . \quad (11)$$

As is evident when taking the scalar product with  $\mathbf{e}$ , the cross product expression represents the component of  $\mathbf{P}$  perpendicular to the respective  $\mathbf{e}$ , i.e. with the component along  $\mathbf{e}$  removed. So we may call  $((\mathbf{e}\mathbf{P})\mathbf{e} - \mathbf{P}) = -\mathbf{P}_T$  with ‘‘T’’ for transverse.

We therefore obtain that the D in Eq 5 is given by

$$D = \mathcal{A} \quad (12)$$

Eq 12 has the typical form of a dissipative parameter related to the integral over the autocorrelation function for a fluctuating quantity[10].

One can also handle more than one noise source by this method. With two independent random fields, along the fixed directions  $\mathbf{e}_1$  and  $\mathbf{e}_2$ , we will have a tensor of the form

$$\overline{\mathbf{X} \otimes \mathbf{Y}} = \mathcal{C}_1 \mathbf{e}_1 \otimes \mathbf{e}_1^\dagger + \mathcal{C}_2 \mathbf{e}_2 \otimes \mathbf{e}_2^\dagger . \quad (13)$$

That is, different noise effects can be added up separately and do not interfere with each other. This is due to the assumed independence of the two noise signals. Note the  $\mathbf{e}_1$  and  $\mathbf{e}_2$  need not be orthogonal.

<sup>1</sup>This is the first point where one uses the properties of the  $\sigma$  as Pauli matrices. Otherwise they could have been any group generators, in which case the cross product formulas are replaced by bilinear products of structure constants [9]

Thus according to Eq 13, for the case of two independent noise signals Eq 9 generalizes to

$$\dot{\mathbf{P}} = [\mathcal{A}_1((\mathbf{e}_1\mathbf{P})\mathbf{e}_1 - \mathbf{P}) + \mathcal{A}_2((\mathbf{e}_2\mathbf{P})\mathbf{e}_2 - \mathbf{P})] . \quad (14)$$

Calling  $(\mathbf{e}_1\mathbf{P})\mathbf{e}_1 - \mathbf{P} = -\mathbf{P}_{\mathbf{T}1}$ , and  $(\mathbf{e}_2\mathbf{P})\mathbf{e}_2 - \mathbf{P} = -\mathbf{P}_{\mathbf{T}2}$  we thus find that the old [14] rotation- decoherence equation Eq 5 now becomes

$$\dot{\mathbf{P}} = \mathbf{P} \times \mathbf{V} - D_1 \mathbf{P}_{\mathbf{T}1} - D_2 \mathbf{P}_{\mathbf{T}2} , \quad (15)$$

with

$$D_1 = \mathcal{A}_1 \quad D_2 = \mathcal{A}_2 \quad (16)$$

Concerning dimensions,  $\mathbf{B}$  is an energy in view of its role in the hamiltonian, and so  $\mathcal{A}$  via Eq 10 is also an energy, which matches the units of  $D$ .

The conclusion Eq 15 could also have been arrived by an intuitive argument where one imagines turning off one noise signal for a short time and then repeating the process with the other noise signal turned off. One would then obtain first the results of Eq 5 with respect to one direction and then with respect to the other direction. The net result would correspond to Eq 15.

As said, the  $\mathbf{e}$ 's can be in any direction, not necessarily orthogonal; and since the independent addition of signals in Eq 13 holds for any number of different signals, evidently Eq 15 can be extended to more than two noise signals by simply adding a  $-D\mathbf{P}_{\mathbf{T}}$  term for each. It is of course essential that the different noise signals be uncorrelated.

The length of  $\mathbf{P}$  is always decreasing with an equation of the type Eq 15 and these considerations can be given an interpretation in terms of the increase of entropy [15]. In particular we note a formula for the decrease of the length of  $\mathbf{P}$  (squared):

$$\frac{1}{2} \frac{d}{dt} \mathbf{P}^2 = \mathbf{P} \cdot \dot{\mathbf{P}} = -\mathbf{P} \cdot (D_1 \mathbf{P}_{\mathbf{T}1} + D_2 \mathbf{P}_{\mathbf{T}2}) = -D_1 \mathbf{P}_{\mathbf{T}1}^2 - D_2 \mathbf{P}_{\mathbf{T}2}^2 , \quad (17)$$

for the case of two independent decoherence or noise signals as in Eq 15.

Concerning the necessity of considering more than one noise source, it is possible or indeed likely that there are noise and decoherence effects on more than one aspect or component of a system. For the SQUID, for example, there might be external flux noise giving fluctuations in  $x^{ext}$  and at the same time effects in the Josephson circuit amounting to fluctuations in  $\beta$ . Such a situation would be described by Eq 15.

With only one noise "axis" the decoherence problem may be viewed as one of random phases or rotations around that axis, as was done in [1] for flux noise in the SQUID. This is sometimes called "dephasing", and  $D$  is the associated diffusion parameter. Thus it may be said that Eq 15 gives the formula for the evolution when there is more than one "dephasing" axis.

## 6 Noise Models

We shall consider different types of noise signals  $\mathcal{N}(t)$ . Noise signals are characterized by their power spectrum  $\mathcal{P}(\omega)$ , which is the fourier transform of the autocorrelation function  $\overline{\mathcal{N}(0)\mathcal{N}(t)}$ , namely  $\mathcal{P}(\omega) = \int_0^\infty dt \cos \omega t \overline{\mathcal{N}(0)\mathcal{N}(t)}$ . One such power spectrum is “white noise” with a cutoff  $\omega_c$ :

$$\mathcal{P}(\omega) = \frac{\omega_c^2}{\omega^2 + \omega_c^2}. \quad (18)$$

This is a constant or white noise spectrum up to frequency  $\omega_c$ , and then falls off as  $1/\omega^2$  at high frequency. This was used in a simplified way in [1]. In section 11 below we will discuss some examples using this kind of noise.

In addition, we also use planckian spectra corresponding to 1, 2, or 3 spatial dimensions. With these we can to try to represent a thermal background and as will be explained below, allows us to conveniently compare cases with and without noise power at zero frequency. They also allow a simple variation of the frequency content by changing  $T$  which is a “temperature ” parameter characterizing the frequency spectrum, with an exponential cutoff above  $\omega \sim T$ . For n=1 we take the planckian form

$$\mathcal{P}(\omega) = \frac{(\omega/T)}{e^{\omega/T} - 1} \quad n = 1. \quad (19)$$

We have fixed the normalizations in Eq 19 and Eq 18 such that  $\mathcal{P}(0) = 1$ . This condition corresponds to setting the time integral of the autocorrelation function equal to one:

$$\mathcal{P}(0) = \int_0^\infty dt \overline{\mathcal{N}(0)\mathcal{N}(t)} = \frac{1}{N} \sum_a \int_0^\infty dt \mathcal{N}^a(0)\mathcal{N}^a(t) = 1, \quad (20)$$

where  $\mathcal{N}^a(t)$  is a particular realization “a” of the signal, and we have generated  $N$  such signals. This convention is particularly convenient since according to Eq 12 the decoherence parameter  $D$  is simply proportional to just this time integral of the autocorrelation function. With this standardized normalization of the noise signal we will regulate its overall strength in different applications by an adjustable small coupling factor.

The planckian forms corresponding to spatial dimensions n=2 and n=3 cannot be normalized in this way since they contain extra powers of  $\omega$ , giving vanishing noise power at  $\omega = 0$ . We therefore choose to normalize them such that the variance of the signals, which is a measure of their magnitude, is equal to that for n=1 at the same T.

This leads to the following definitions

$$\begin{aligned} \mathcal{P}(\omega) &= \frac{\pi^2}{12 \zeta(3)} \frac{(\omega/T)^2}{e^{\omega/T} - 1} & n = 2 \\ &= \frac{5}{2\pi^2} \frac{(\omega/T)^3}{e^{\omega/T} - 1} & n = 3. \end{aligned} \quad (21)$$



The variance of the signal corresponds to the integral over the power spectrum, so with these normalizations the integral  $\int_0^\infty d\omega \mathcal{P}(\omega)$  is the same for all three signals in Eq 19 and Eq 21.

Specifically, one finds

$$\overline{\mathcal{N}^2} = \frac{2}{\pi} \int_0^\infty d\omega \mathcal{P}(\omega) = T \frac{\pi}{3} \quad (22)$$

For  $T=0.025$ , which we shall use in many of the simulations, this gives a typical signal strength of  $\sqrt{\overline{\mathcal{N}^2}} = 0.16$ . As we shall see below in section 10, the case of noise signals with the property  $\int_0^\infty dt \overline{\mathcal{N}(0)\mathcal{N}(t)} = 0$ , as in Eq 21, are of special interest.

To numerically generate a particular signal  $\mathcal{N}^a(t)$  as a realization of one of the above models, we work with a discretized fourier space where  $\mathcal{N}(t) = \sum_\omega \mathcal{N}_\omega e^{i\omega t}$ . A given random set  $a$  of the  $\mathcal{N}_\omega$  then determines the signal. We have used two procedure to generate the  $\mathcal{N}_\omega$ .

In the random phase procedure, one takes  $\sqrt{\mathcal{P}(\omega)}$  times a random phase  $e^{i\theta}$  with  $\theta$  chosen randomly and uniformly in the interval  $0 \geq \theta \geq 2\pi$ .

In the gaussian modulus method one chooses a real and imaginary part of  $\mathcal{N}_\omega$  randomly from a gaussian distribution with zero mean and variance  $\mathcal{P}(\omega)$ . Both methods lead to an ensemble with the power spectrum  $\sim \mathcal{P}(\omega)$ . We find that both procedures lead to very similar results in our simulations.

Figure 2 shows some samples of the different noise signals. The upper curve is for Eq 18. One sees the presence of the high frequency tail in the power spectrum. The middle curve is for the planckian  $n=3$ , Eq 21, and the lower curve for the planckian  $n=1$ , Eq 19. These latter two differ in that for  $n=3$  there is no power at zero frequency, while for  $n=1$  it is present. The temperature  $T=0.025$  or  $\omega_c$  is the same for all three. It will be seen that the amplitude of the signals is roughly in accord with Eq 22, with  $\sqrt{\overline{\mathcal{N}^2}} = 0.16$ .

## 7 Relation Between $H_{\mathcal{N}}$ and $\mathbf{B}$

In this section we determine the relations between the random  $\mathbf{B}$  of the two-state description Eq 2 and the noise term in the full hamiltonian Eq 1. Given these relations, we will be able to compare the results of a full numerical simulation with Eq 1 and the analytical predictions from Eq 12.

As explained below, noise in the ‘z’ direction arises through fluctuations in  $x^{ext}$ , and in the ‘x’ direction, fluctuations in  $\beta$ . In the case of the SQUID these correspond to noise/decoherence in the external flux and in the junction circuit, respectively. It is quite plausible that they should correspond to independent noise sources.

### 7.1 Noise in the “z-direction”

We thus consider adding a noise term representing a fluctuation of  $x^{ext}$  in Eq 1:

$$H_{\mathcal{N}} = \delta x^{ext} V_o x = \delta \eta \mathcal{N}(t) V_o x . \quad (23)$$

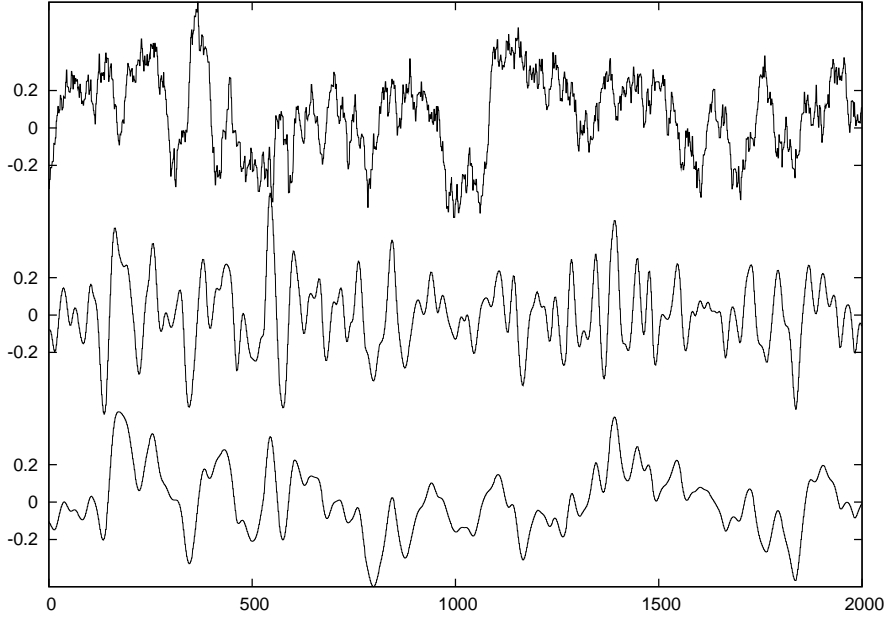


Figure 2: Samples of noise signals  $\mathcal{N}(t)$ . Upper curve: Cut-off white noise from Eq 18 with cutoff  $\omega_c = 0.025$ . Middle curve: planckian noise for  $n=3$  as in Eq 21 with  $T=0.025$ . Lower curve: planckian noise for  $n=1$  as in Eq 19 with  $T=0.025$ . The signals are normalized to have the same variance or integrated noise power but differ in having zero (middle) or non-zero (upper and lower) noise power at zero frequency. The high frequency tail present in the power spectrum of the upper, non-planckian, curve is evident. With  $L = 400pH$  and  $C = 0.1pF$  for the SQUID, the time unit in this and all further plots would be  $6.3 \times 10^{-12} sec$ .

We call the fluctuation  $\delta x^{ext}$  and for a particular noise signal "a" it is represented by  $\delta\eta \mathcal{N}^a(t)$  with  $\delta\eta$  an overall coupling strength. By using the identification  $x \approx x_c \sigma_z$  (see section 3) connecting the operator  $x$  of the full hamiltonian with the  $\sigma$  of the spin 1/2 picture, one sees that this  $H_{\mathcal{N}}$  is equivalent [5] to the B field of the two-state model as :

$$B_z = 2V_0 x_c \delta\eta \mathcal{N} , \quad (24)$$

with other B components zero. We therefore predict, according to Eq 12, that when using a noise signal normalized with  $\mathcal{P}(0) = 1$  as explained in section 6, a decoherence constant from the full simulation with Eq 1

$$D = \int_0^\infty \overline{B_z(0)B_z(t)} dt = 4(V_0 x_c \delta\eta)^2 = 0.89 \times 10^3 (\delta\eta)^2 , \quad (25)$$

where in the last step we insert  $V_0 = 16.3, x_c = 0.9$ .

## 7.2 Noise in the “x-direction”

Switching to the “x-direction”, we consider the effect of small variations of  $\beta$  in Eq 1, amounting to fluctuations in the barrier potential. Since  $\beta$  regulates the tunneling, a change in  $\beta$  induces a change in the tunneling energy. Thus in the two-state hamiltonian Eq 2 a variation in  $\beta$  induces (apart from an unimportant constant shift) a change in the  $\sigma_x$  term, a  $B_x$ . Other components of  $\mathbf{B}$  are zero.

To obtain the magnitude of  $B_x$  [12], one notes that the coefficient of  $\sigma_x$  is the tunnel splitting;  $V_x + B_x = \omega_{tunnel} + \delta\omega_{tunnel}$ . Thus  $B_x = \delta\omega_{tunnel} = \delta\beta \frac{d\omega_{tunnel}}{d\beta}$ .

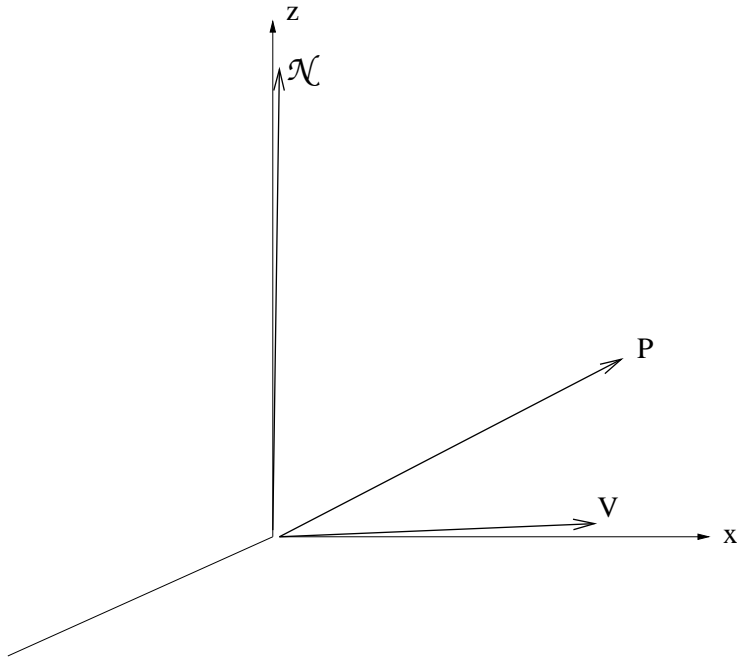


Figure 3: Typical configuration of vectors used in the simulations. With no damping the polarization vector  $\mathbf{P}$  rotates around  $\mathbf{V}$ , so with  $\mathbf{V}$  in the x-direction there are oscillating components  $P_z, P_y$ . For  $D$  not too large these are damped oscillations as the component of  $\mathbf{P}$  perpendicular to the noise direction  $\mathcal{N}$  or  $\mathbf{B}$  is reduced. For very strong  $D$ ,  $\mathbf{P}$  is “pinned” along the noise vector, corresponding to the “Collapse of the Wavefunction”. The initial  $\mathbf{P}$  is of unit length and along the z-axis for Figs 5 and 6, while for Fig 7 it lies at 45 degrees in the x-z plane.

Although there are analytic methods of evaluating tunneling energies, they involve exponentially sensitive effects and it seems best to find  $\frac{d\omega_{tunnel}}{d\beta}$  from our previous numerical results. In the vicinity of  $\beta = 1.19$ , (and with  $V_0 = \mu = 16.3$  where we carry out our simulations) examination of Table II of [1] yields  $\frac{d\omega_{tunnel}}{d\beta} \approx -0.18$  near  $\beta = 1.19$ . Thus, for fluctuations around  $\beta = 1.19$  the  $\mathbf{B}$

field associated with a change in  $\beta$  is

$$B_x = \delta\beta \frac{d\omega_{tunnel}}{d\beta} = (-0.18)\delta\beta = (-0.18)\delta\beta_o \mathcal{N}, \quad (26)$$

We write the fluctuations in  $\beta$  as  $\delta\beta = \delta\beta_o \mathcal{N}$ , with  $\mathcal{N}$  one of our noise signals and  $\delta\beta_o$  a strength parameter. According to Eq 12, when  $\mathcal{N}$  has the integral of the autocorrelation function normalized to one,

$$D = 0.032 \delta\beta_o^2. \quad (27)$$

For the numerical calculations, we wish to insert the same  $\delta\beta$  fluctuations in Eq 1. Since  $x^2/2$  is the leading term in  $\cos x$  which contributes to the level splitting, a small variation in  $\beta$  can be adequately represented by adding a term  $\delta\beta V_o x^2/2$  in the full hamiltonian. We thus should set, in Eq 1

$$H_{\mathcal{N}} = -\delta\beta V_o \frac{1}{2}x^2 = -\delta\beta_o \mathcal{N} V_o \frac{1}{2}x^2. \quad (28)$$

### 7.3 Comparison of x and z-noise

Our two examples of ‘z-noise’ and ‘x-noise’ are instructive in that the effective B fields for the two-state system Eq 24 and Eq 26 and the associated D’s, Eq 25 and Eq 27 differ widely for similar noise signals. The difference originates in the fact that the ‘z-noise’ operator is linear  $\sim x$ , while the ‘x-noise’ operator is quadratic  $\sim x^2$ . The two lowest states comprising our two-state system have, with  $x^{ext} = 0$ , odd or even parity. Thus they will be strongly connected by the parity odd  $x$  operator. For the  $x^2$  operator on the other hand the change in the energy splitting is only due to the different shifts of the two states under  $x^2$  and so is much smaller. For  $x^{ext} \neq 0$  but small the situation will be qualitatively similar.

Thus the symmetry properties associated with the noise or decoherence can be important. With specific devices this may suggest a choice of operating conditions where the effects can be minimized.

## 8 Tests by Numerical Simulation

We turn to numerical tests of the formalism and the above results Eq 25 and Eq 27 of the spin- $\frac{1}{2}$  picture. We check them against results from the full hamiltonian Eq 1 with the corresponding  $H_{\mathcal{N}}$ , namely Eq 23 or Eq 28, inserted in the hamiltonian. We find the decoherence parameter D from a fit to the damping of  $|\mathbf{P}|$  in the numerical calculations and compare it with the analytic predictions. For our various tests we chose a coupling  $\delta\eta$  such that the decoherence time  $1/D$  is on the order of some thousands of time units. For the typical SQUID parameters of mentioned in the introduction this corresponds to a decoherence time in the tens of nanoseconds.

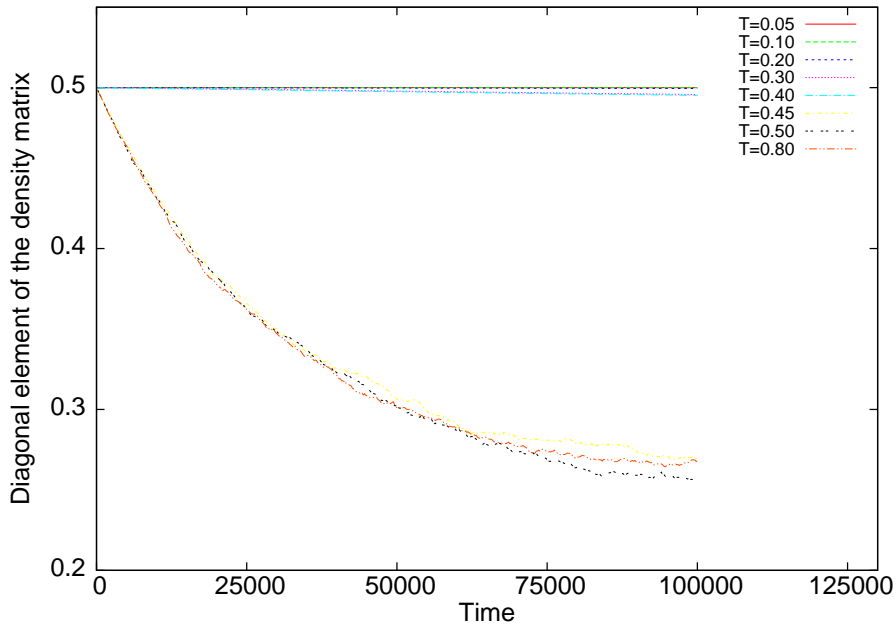


Figure 4: Excitation to higher states. When the noise power spectrum contains frequencies above that of the principal level spacing, here 0.4, the diagonal elements of the 2x2 density matrix fall below 1/2. When it does not contain these frequencies the relaxation is to 1/2.

## 8.1 Parameter Ranges

There will be certain conditions on the range of parameters where the analytical arguments can be applied.

One condition concerns large perturbations, where the nature of the system is changed substantially. These are evidently beyond the scope of the theoretical method, and would have to be dealt with simply by simulation alone. This is particularly relevant in our example of  $\beta$  fluctuations or ‘x- noise’ where the tunneling energy is very small and  $\beta$  fluctuations have a relatively large effect. This is discussed in sect.8.4.

A second condition concerns the frequency spectrum of the noise, as characterized by the  $T$  or the  $\omega_c$  of the noise power spectra. If the dominant noise frequencies are too low, on the order of, or less than the important frequencies of the system, this is in contradiction to our assumption that the system can be taken as constant over many cycles of the noise [13]. In sect 11 we shall discuss some features of low frequency noise. On the other hand, if the frequencies in the noise are too high, one risks exciting higher states and so violating our assumption of an effective two-state system. Since the important system frequency we deal with is  $\omega_{tunnel} = 0.0044$ , and the distance to the next set

$\mathbf{V}$	$\mathbf{P}_{\text{initial}}$	$D$
(0.0044, 0.0, 0.0)	(1,0,0)	0.00134
(0.0044, 0.0, 0.0)	(0,0,1)	0.00122
(0.0044,0.0,0.006)	$(1, 0.0, -1)\frac{1}{\sqrt{2}}$	0.00118
(0.0044,0.0,0.02)	(1,0,0)	0.00141

Table 1: Study of the constancy of  $D$  for various starting conditions. A  $n=1$  planckian noise in the ‘z-direction’ with  $T = 0.05$  is used. The coupling is  $\delta\eta = 0.00128$ , for which the prediction Eq25 is  $D = 0.00146$ . In the first two entries  $\mathbf{V}$  is along the x-axis while the starting  $\mathbf{P}$  is first along the x-axis and in the second line along the z-axis. In the third entry  $\mathbf{V}$  is close to 45 degrees with the z-axis and  $\mathbf{P}$  starts orthogonal to it in the lower hemisphere. In the last and fourth entry  $\mathbf{V}$  makes an angle of only 12 degrees with the z-axis and  $\mathbf{P}$  starts along the x-axis. One observes that at about the 20% level the value of  $D$  is the same for the various examples and near to the predicted value. The notation for the vectors refers to  $(x, y, z)$ .

of levels is about 0.4, one has the condition  $0.0044 \ll T, \omega_c \ll 0.4$ . This criterion applies of course for our typical configurations and would have to be adjusted for others.

The excitation to higher states above that of our effective two- level system can be detected in that the diagonal elements of the 2x2 density matrix will relax not to 1/2, but to some smaller value, reflecting the missing probability. We can perform an amusing numerical experiment on this by using a ‘rectangular’ noise power spectrum  $\mathcal{P}(\omega)$  which is exactly zero above some  $\omega = T$ . The resulting behavior of the density matrix is shown in Fig 4 for various values of  $T$ .

If the noise power does not contain frequencies equal or higher than those needed to go to the next set of states, the density matrix should relax to 1/2. With our typical parameters, this frequency is about 0.4. In Fig 4 it is seen that when the maximum noise frequency is below this value the relaxation is indeed to 1/2. With higher frequencies present the relaxation is to less than 1/2. (That it falls to 1/4 reflects the fact that the numerical calculations were carried out in a 4-state basis.)

Although our various noise power spectra do not have a simple rectangular cutoff, we anticipate a similar behavior with our exponentially cutoff planckian spectra. We do indeed find with low  $T$ 's and couplings that are not too strong that calculations performed with a two-state basis give the same results as basis with more states, indicating that the excitation of higher states is not important. The results we present below are always under these conditions.

## 8.2 State Independence of $D$

Probably the most striking aspect of the theory is that, with the given assumptions, the effect of the environment, here represented by the noise, can be

$\mathbf{V}$	$T$	$D$	$\rho_{11}$
(0.0044, 0.0, 0.0)	0.0125	0.0011	0.50
	0.025	0.00128	0.50
	0.05	0.00132	0.50
	0.10	0.00145	0.50
	0.20	0.00157	0.45

Table 2: Temperature dependence of the decoherence parameter  $D$  determined from the numerical simulations using noise signals in the ‘z- direction’ with the power spectrum Eq 19 and coupling  $\delta\eta = 0.00128$ . According to Eq 25,  $D$  should be temperature independent and have the value 0.00146. The final value of the density matrix element  $\rho_{11}$  should be  $\frac{1}{2}$  if there is no excitation of higher states above the effective two-state system. The last entry for  $\rho_{11}$  shows some deviation from this as  $T$  approaches the principal level spacing 0.4.

represented by a single parameter  $D$ . Most importantly,  $D$  does not depend on the state of the system. This means that Eq 5 is a *linear* equation for  $\mathbf{P}$ . This would not be the case, for example, if one had  $D = D(P)$ . Linearity for the evolution of the density matrix is a general result of quantum mechanics and it is non-trivial that our approximate method respects this.

We can provide some tests of this feature in the full numerical simulation. One may take a given noise signal with a given coupling and determine  $D$  for different configurations of the potentials and of the initial state. In Table 1 we show some examples, using ‘z-noise’ with the parameter  $\delta\eta = 0.00128$ , for which, according to Eq 25, the prediction is  $D=0.00146$ .

The first two entries are for symmetric potentials,  $x^{ext} = 0$ , that is with  $\mathbf{V}$  in the x-direction. For the first line the system is started with  $\mathbf{P}$  also in the x-direction, that is with a wavefunction which is a linear combination of equal wavepackets in the left and right potential wells. In the second line the system is started with  $\mathbf{P}$  in the z-direction, corresponding to the initial wavefunction concentrated in only one potential well. In the next two entries we show the case of some asymmetric potentials, so that  $\mathbf{V}$  lies at some angle in the x-z plane. In the third line  $\mathbf{V}$  is at a 45 degree angle, and in the fourth line close to the z-axis at a 12 degree angle.

### 8.3 Test for ‘z-noise’

We now examine the nature of the evolution with “noise along the z-axis”. With  $\mathbf{V}$  along the x-axis, Fig 3 shows this situation with  $\mathbf{P}$  in some general direction.

In a first test we start  $\mathbf{P}$  along the z-direction again with coupling  $\delta\eta = 0.00128$ . One anticipates that  $\mathbf{P}$  will rotate around the x-axis while its length decreases. Inserting Eq 23 in Eq 1, evaluating the density matrix and extracting  $\mathbf{P}$  one finds the results shown in Fig 5. The left panel shows the projection of  $\mathbf{P}$  on the z-axis, with the expected damped oscillations. The right panel shows

the decrease of the total length of  $\mathbf{P}$ .

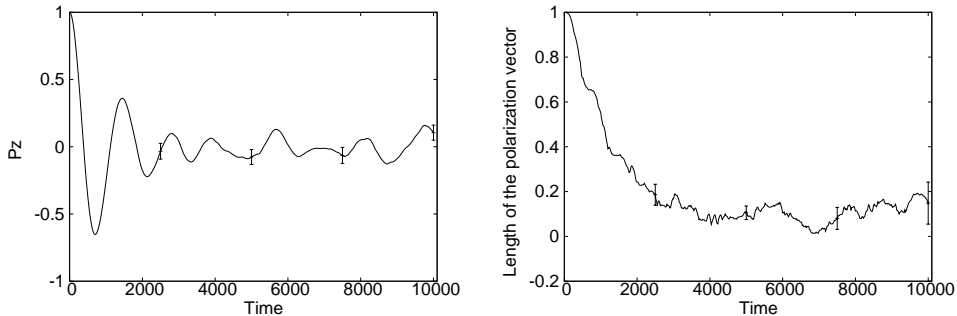


Figure 5: Simulation with Eq 1 using “z-noise” due to  $x^{ext}$  fluctuations as given by Eq 23. The configuration corresponds to Fig 3 with  $\mathbf{P}$  started along the z-axis. Left: Projection of  $\mathbf{P}$  on the z-axis showing damped oscillations. Right: Damping of the total length of  $\mathbf{P}$ . A fit for the length with  $e^{-Dt}$  yields  $D = 0.00132$ , while the prediction from Eq 25 is  $D = 0.00146$ . The error bars indicate the dispersion of values expected for an average made from  $N$  samples, namely  $\frac{1}{N} \sqrt{\sum_1^N (P_a - \bar{P})^2}$ , where  $P_a$  is the quantity being plotted, resulting from a given noise signal ‘a’.

The value of  $D$  emerging from the simulation is found by fitting  $e^{-Dt}$  to the curve of the right panel, yielding  $D=0.00132$ . On the other hand the prediction from Eq 25 is  $D=0.00146$ . Thus there is good agreement.

These plots were produced using the  $n=1$  planckian noise Eq 19. It is a feature of the prediction Eq 25 with fixed  $\delta\eta$  that the  $D$  resulting from the simulation should be given by  $\mathcal{P}(0)$  and independent of  $T$ , even though a change of  $T$  implies a change in the frequencies present in the noise.

To test this, Table 2 shows the values of  $D$  resulting from various  $T$ 's used in simulations with  $n=1$  planckian noise. The first and last values of the temperature are near the margins of the allowed region  $0.0044 \ll T, \omega_c \ll 0.4$ . One observes approximate agreement with the analytic prediction  $D=0.00146$ . At the highest temperature the excitation to states above the lowest two states manifests itself in the relaxation of the density matrix element to a value less than  $\frac{1}{2}$ .

These results are meant simply as a check on our numerical and mathematical methods and should not be taken to mean that the decoherence is temperature independent. To the contrary, a temperature dependence is rather to be expected. With the normalizations we have adopted, it would be represented by a temperature dependence of the coupling parameter  $\delta\eta$ .

## 8.4 Test for ‘x-noise’

Fluctuations in  $\beta$  correspond to changes in the tunneling energy, a  $\sigma_x$  operator in our notation. As was discussed in section 7.3, fluctuations in  $\beta$  have relatively



small effects compared to similar fluctuations in the  $x^{ext}$  parameter, leading to a much smaller  $D$  for  $\beta$  fluctuations or ‘x-noise’.

If for the purpose of comparing the analytic and numerical predictions, we were to increase the coupling constant  $\delta\beta_o$  in the simulations, there is the difficulty that using a larger  $\delta\beta$  will induce substantial changes in the small tunneling energy, violating our assumption that the fluctuations do not essentially change the system. For example, we work with  $V_x = \omega_{tunnel} = 0.0044$ , and according to Eq26 the  $B_x$  induced by a  $\delta\beta$  is  $(-0.18)\delta\beta_o\mathcal{N}$ . If we wish to have  $B_x \ll 0.0044$  with the typical size of noise signals 0.16 (see sect.6), then we require  $\delta\beta_o \ll 0.01$ , which implies  $D$  on the  $10^{-6}$  level, according to Eq 27.

While such small effects can be unstable and difficult to detect numerically, we show in Fig6 a run for  $x^{ext} = 0$  with the coupling  $\delta\beta_o = 0.01$ . The temperature for  $n=1$  planckian noise was set to  $T=0.05$ . A fit gives  $D = 5 \times 10^{-6}$ , while the prediction of Eq27 is  $D = 3 \times 10^{-6}$ . Although there is qualitative agreement, it is evidently not so precise as in the case of the z-noise. This may be due to our various approximations as well as numerical uncertainties.

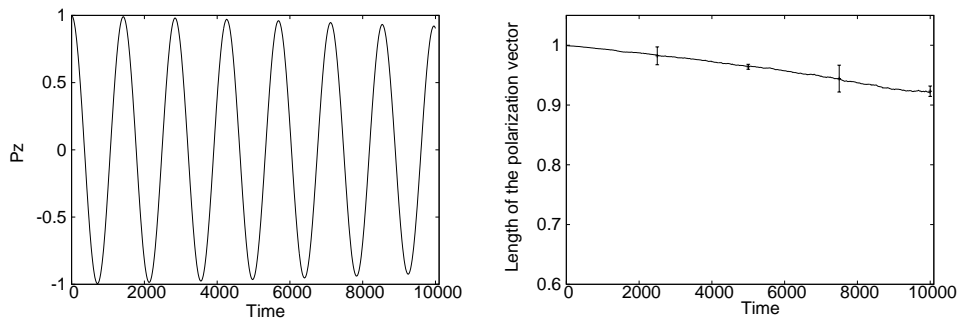


Figure 6: Relaxation due to  $\beta$  fluctuations or “x-noise”. Left: Projection of  $\mathbf{P}$  on the z-axis. Right: Damping of the total length of  $\mathbf{P}$ . For the configuration of Fig3 with  $\mathbf{P}$  started along the z- axis. A fit to the length with  $e^{-Dt}$  yields  $D = 5 \times 10^{-6}$ , while the prediction from Eq25 is  $D = 3 \times 10^{-6}$ . A weak coupling  $\delta\beta_o = 0.01$  implying weak damping must be used to avoid a large shift  $\delta\omega_{tunnel}/\omega_{tunnel}$ .

## 9 “Collapse” and “Watched Pot”

Since the beginnings of quantum mechanics the “Collapse of the Wavefunction” has been assumed to be an instantaneous and somewhat mysterious process, not describable in a physical manner. However, as was noted in the beginning of studies of decoherence [14], the action of the external influences, here simulated by the noise, may be quantitatively examined and the induction of a “Collapse of the Wavefunction”-like behavior of the system studied. This occurs through the effect of the  $-DP_T$  term, which tends to eliminate off-diagonal matrix elements of the density matrix and so to reduce the density matrix to a clas-

sical probability distribution, an incoherent mixture of the states of a definite “quality”, the eigenstates of  $\sigma_z$ .

As the external influence, represented by  $D$ , becomes very strong, the “Collapse of the Wavefunction” occurs very rapidly. In addition, the further evolution of the system is inhibited and in the limit can be essentially stopped completely [14]—much like the ‘fixing’ of the state by a ‘measurement’. This is the “Turing” or “Watched Pot” effect. In terms of Eq 5 this occurs because the large  $D$  “pins”  $\mathbf{P}$  to the noise axis so there is a very small  $P_T$  and very little subsequent damping.

## 9.1 Strong Damping with $\mathcal{N}$ , $\mathbf{V}$ Perpendicular

With our present system we can illustrate and study such effects quantitatively. Let the initial  $\mathbf{P}$  be chosen to have length one (pure state) and be oriented at an angle such that both  $P_z$  and  $P_x$  components are substantial. Fig 3 indicates such a starting condition. If there is a strong noise along the  $z$ -axis,  $P_x$  will rapidly disappear: there is a “Collapse of the Wavefunction” to an incoherent mixture of “up” and “down” states. After this “collapse” the large value of  $D_z$  inhibits further evolution—the “Watched Pot” effect.

Fig 7 shows a simulation for such conditions. The length of  $\mathbf{P}$  is plotted. One observes a rapid decrease of the length until only the original  $P_z$  survives. The wavefunction “collapses” in a very short time. After this, the length remains “frozen” to this value—the “Watched Pot” effect. Increasing  $D$  gives a faster “collapse” and a stronger “watching”. As with the other simulations, the full hamiltonian Eq 1 is used here.

The parameter characterizing “strong” or “weak” damping is the ratio  $D/\omega$ , where  $\omega = V$  is the energy splitting of the two levels or the magnitude of  $\mathbf{V}$ . This follows from Eq 5, where dividing through by  $V$  yields a dimensionless time parameter  $t\omega$  and the parameters  $D/\omega$ . For small  $D/\omega$  one has weakly damped precession of the  $\mathbf{P}$  vector around  $\mathbf{V}$ . For  $D/\omega \gg 1$  one enters the “Watched Pot” regime.

Examination of the solutions of Eq 5 for  $\mathbf{V}$  in the  $x$ - direction with  $V_x = \omega_{tunnel}$  and  $\mathbf{P}$  initially in the  $z$ - direction leads to the behavior [14]

$$P_z \approx e^{-t(V_x^2/D)} \quad (29)$$

for  $\mathbf{P}$  initially along the  $z$ -axis. This result follows from combining the  $z$  and  $y$  components of Eq 5 to give the equation  $\ddot{P}_z + D\dot{P}_z + V_x^2 P_z = 0$  and solving for large  $D$  [11]. For very large  $D$  the graph in Fig 7 will decrease extremely slowly (see Fig 6 of [1]).

## 9.2 Strong Damping with $\mathcal{N}$ , $\mathbf{V}$ Nearly Parallel

In the above case  $\mathcal{N}$  or  $\mathbf{B}$  and  $\mathbf{V}$  were at right angles. This is the usual “Watched Pot” configuration as it has been studied for chiral molecules, neutrinos, or the SQUID with a symmetric potential and dominant flux noise [14] [1]. In

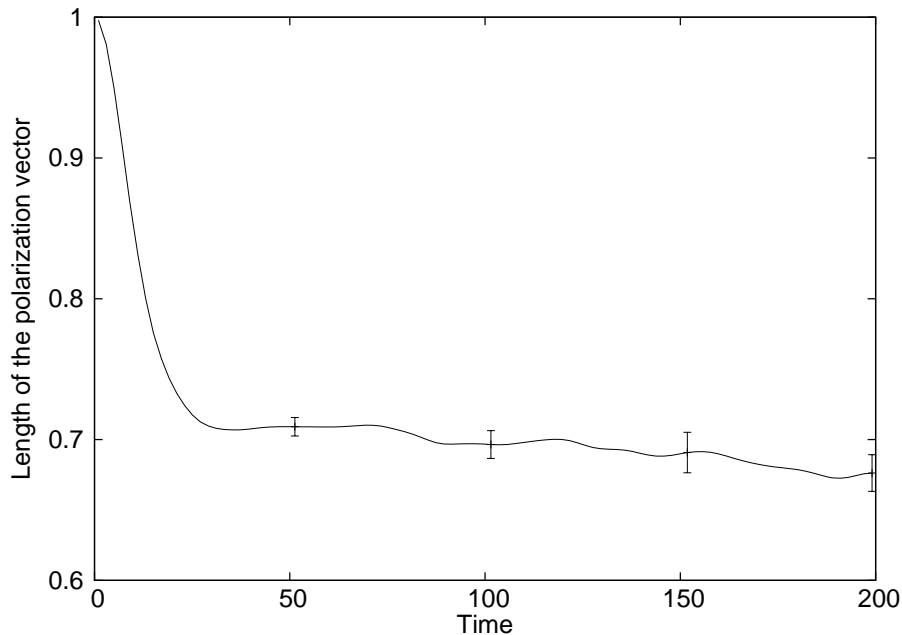


Figure 7: The “Collapse of the Wavefunction” followed by the “Watched Pot” effect. The plot shows the evolution of the length of  $\mathbf{P}$  for the configuration of Fig3 with the initial  $\mathbf{P}$  of length one and at 45 degrees in the x-z plane. The  $P_x$  component “collapses” to zero quickly, giving an incoherent mixture of “up” and “down” states. This is then followed by a near “freezing” of the evolution. These effects result from the strong noise (or “measurement”), here with  $D/\omega \approx 100$ . Note the short time scale, the time unit is the same as in the other plots, namely with  $L = 400pH$  and  $C = 0.1pF$  for a SQUID, the unit is  $6.3 \times 10^{-12} sec$ .

all these cases one has— or it is assumed—, that the observable “quality” in question (chirality, flavor, flux state) is conserved in the interaction with the environment. Since we take this ‘quality’ to be represented by an eigenstate of  $\sigma_z$ ,  $\mathbf{B}$  is necessarily in the z-direction.

However, one may also envision the opposite situation where  $\mathcal{N}$  and  $\mathbf{V}$  are in the same direction. This would be the case, for example, with a strongly asymmetric potential for the SQUID ( $x^{ext} \neq 0$ ) and dominant flux noise. (This appears to be the case for the experiment mentioned in ref [13].)

In this case the analog to Eq 29 for the long term behavior of the parallel component after the perpendicular components have been “collapsed” is found to be

$$P_{parallel} \approx P_{parallel}^o e^{-t \frac{DV_z^2}{V^2 + D^2}}. \quad (30)$$

$P_{parallel}^o$  is the component remaining after the initial “collapse” and  $V^2$  the square of  $\mathbf{V}$ . This result follows from writing Eq 5 as a set of linear equa-

tions, taking  $\mathbf{P} \sim e^{-\lambda t}$  and solving the determinantal equation for the smallest eigenvalue  $\lambda$ .

For  $D \gg V$  one recovers Eq 29. For  $D \ll V$  there is a new regime with a suppression due to the large value of  $V$ , with the behavior  $\sim e^{-tD\theta^2}$  where  $\theta = V_x/V$ . Naturally in the limit where  $\mathbf{V}$  and  $\mathcal{N}$  are exactly parallel,  $\mathbf{P}$  will remain constant, as one sees setting  $V_x = 0$  in Eq 30.

## 10 Vanishing Noise Power at Low Frequency

In the numerical work so far we have assumed that the time integral of the autocorrelation function, or equivalently  $\mathcal{P}(0)$ , is non-zero. However a very interesting special case occurs when it is in fact zero as for Eq 21. Then Eq 16 implies

$$D = 0 \quad \int_0^\infty \overline{B(0)B(t)} = 0 \quad (31)$$

To check if Eq 31 holds with the full hamiltonian we perform simulations comparing noise signals with planckian power spectra for  $n=1$  and  $n=3$ . If Eq 31 indeed holds there should be little or no relaxation in the  $n=3$  case. Since our different signals have been normalized in Eq 19 and Eq 21 to have the same variance  $\overline{\mathcal{N}^2}$ , and the square root of the variance is the typical size of the signal, our comparison is with signals of the same ‘strength’.

Employing these signals for noise in the  $z$  direction in Eq 23, we obtain the results shown in Fig 8. The configuration is as in Fig 3 with  $\mathbf{P}$  started in the  $z$ -direction and the parameters the same as for Fig 5. The left panel of Fig 8 is for  $n=1$  noise and shows the expected relaxation of  $P_z$ . The right panel is for  $n=3$  and shows no apparent decoherence or damping effect in the oscillations of  $P_z$ .

An examination of the length of  $\mathbf{P}$  shows that while it goes to zero for  $n=1$ , for  $n=3$  it declines by only about 1% over the length of the run.

Thus despite the at first sight similar appearance of the lower two signals in Fig 2 there is a great difference in the decoherence they induce and the expectation from Eq 31 is indeed verified in full calculations with Eq 1. The exact vanishing of  $D$  in Eq 31 is presumably a consequence of the use of second order perturbation theory in the derivation and should be lifted in higher order. A similar run for  $n=2$  shows in fact some weak decoherence, with  $D$  at the  $\sim 10^{-5}$  level, perhaps indicative of the higher order effects.

## 11 Very Low Frequency Noise

Eq 5 gives a local-in-time description in terms of a single “frictional” or “dissipative” constant  $D$ .  $D$  does not depend on the state of the system (the value of  $\mathbf{P}$ ) or on the internal hamiltonian (the value of  $\mathbf{V}$ ).  $D$  depends only on the properties of the noise, and our simulations have quantitatively verified this. This simple structure has its origin in the “random walk” behavior of

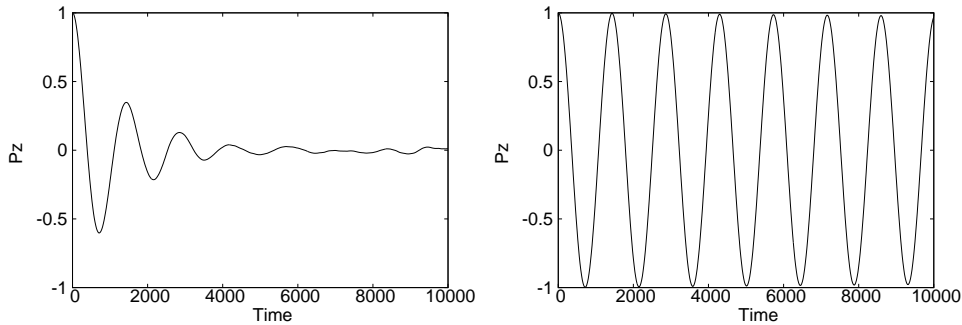


Figure 8: Identical runs for  $P_z$  but with two kinds of noise. Left: Planckian noise power spectrum with  $n=1$  (lower curve of Fig 2), having non-zero power at zero frequency. Right: Planckian noise power spectrum with  $n=3$ , having zero power at zero frequency (middle curve of Fig 2). The two noise signals are adjusted so as to have the same variance or integrated noise power. There is a striking difference in the damping or decoherence, even though the equality of variances assures signals of the same “strength”. The conditions are the same as for Fig 5.

the integral of the noise signal  $\int_0^t B(t')dt'$ . If  $B$  is a random variable then its integral represents a random walk and, as was used in arriving at Eq 10, one has  $(\int_0^t B(t')dt')^2 = 2t\mathcal{A} = 2tD$ , with  $\mathcal{A}$  the time integral of the autocorrelation function of the noise. This is the result of a random walk with steps given by  $\sqrt{2\mathcal{A}}$ . Therefore  $\int_0^t B(t')dt'$  is gaussian distributed with a variance increasing in time as  $\sim t$ , which finally leads to the exponential in time  $\overline{P} = e^{-Dt}$ .

If, however, the noise is dominated by very low frequencies [13] such a local-in-time description is not relevant and the methods presented in the above discussions should not be expected to apply. For times  $t$  small compared to the time scale on which the noise  $B$  varies,  $\int_0^t B(t')dt'$  is not undergoing a random walk. Indeed, in the limit a particular realization  $B^a(t)$  may be taken as effectively constant and one has  $\int_0^t B^a(t')dt' = tB^a(0)$  instead of the  $t^{1/2}$  random walk. The decoherence will now result from the average over the different  $B^a(0)$ .

A simplest case to analyze in this way is that of subsection 7.2 where the noise vector  $\mathbf{B}$  is parallel to  $\mathbf{V}$  (junction circuit noise for the SQUID).  $\mathbf{V}$  gives the rotation rate of  $\mathbf{P}$  in the z-y plane for a  $\mathbf{P}$  started along the z-axis. Thus  $V \rightarrow V + B$  with random  $B$  gives a spread of the orientation of the  $\mathbf{P}$  increasing in time and so a decreasing length of the averaged  $\mathbf{P}$  or decoherence according to

$$\overline{P} = \overline{\cos \int_0^t B(t')dt'} \approx \overline{\cos B(0)t} = \int \cos Bt \text{Prob}(B)dB \quad t \ll t_{noise} \quad (32)$$

where  $t_{noise}$  is the time scale over which  $B$  changes and  $\text{Prob}(B)$  is the probability distribution for the  $B$ . With a gaussian  $\text{Prob}(B)$  one obtains  $\overline{P} = e^{-(1/2)\overline{B^2}t^2}$ . In general for small times one will expect  $\overline{P} \approx 1 - \frac{1}{2}\overline{B^2}t^2$ .

One sees that when  $t \ll t_{noise}$  the relevant quantity is the magnitude of the fluctuations of  $\mathbf{B}$ , namely  $\overline{B^2}$ . As is evident, for example, in the discussion around Eq 22, this is not the same as the  $\mathcal{P}(\omega = 0)$  entering into  $D$ . Rather  $\overline{B^2}$  is given by the integral over  $\mathcal{P}(\omega)$ , Eq 22.

In Fig 9 we show the result of some simulations with very low frequency x-noise compared to a high frequency case.

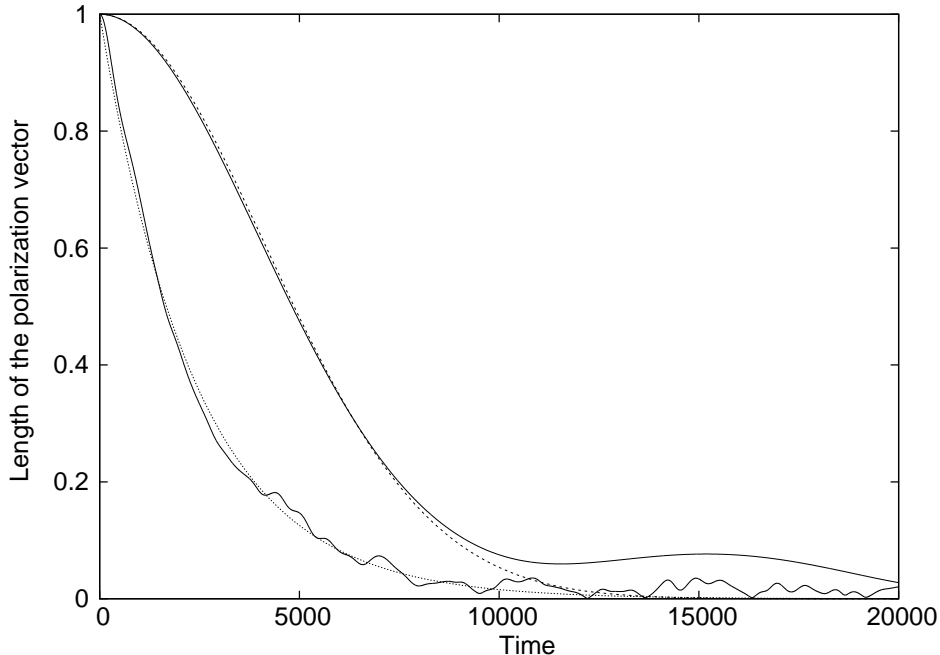


Figure 9: Simulations with low and high frequency x-noise compared. The upper curve shows the effect of a “rectangular” noise power spectrum with cutoff  $\omega_c = 2 \times 10^{-4}$  and the lower with  $\omega_c = 1 \times 10^{-2}$ . The low frequency case exhibits the expected  $\overline{P} \sim e^{-const.t^2}$  behavior and the high frequency case the  $\overline{P} \sim e^{-const.t}$  behavior of our main discussion. The dashed and dotted lines are fits for the two types of behavior.

We use a cut-off white noise spectrum similar to Eq 18. However to make the situation with the noise frequencies completely clear we use a “rectangular” spectrum with  $\mathcal{P} = 1$  up to  $\omega_c$ , where it is then abruptly cut off. The typical time  $t_{noise}$  characterizing a change in a noise signal is then less than or on the order of  $\omega_c$ . The upper curve is for the small  $\omega_c = 2 \times 10^{-4}$  or  $t_{noise} > 5000$ . In order to make the effects evident the relatively large value  $\delta\eta = 0.1$  was used. The behavior  $\overline{P} \sim e^{-const.t^2}$  is seen and a fit (dashed line) gives  $2.0 \times 10^{-8}$  for the constant. Using Eq 26 to find the effective  $B$ , and the integral over the power spectrum to find the variance, one predicts  $const. = (1/2)\overline{B^2} = 2.9 \times 10^{-8}$ , in reasonable agreement. The lower curve, on the other hand, is with the higher frequency noise  $\omega_c = 1 \times 10^{-2} = 1/100$ . One observes the simple exponential

behavior (dotted line), with the coefficient  $D = 4.1 \times 10^{-4}$  in approximate agreement with formula Eq 25 for  $D$  which gives  $D = 3.2 \times 10^{-4}$ . That the low frequency case has the smaller effective decoherence in this example is due to the fact that with the “rectangular” noise spectrum and  $\mathcal{P}$  fixed to one below  $\omega_c$ , the variance  $\overline{B^2}$  decreases as  $\omega_c$  decreases (Eq 22). While for the purposes of comparison we have kept  $\mathcal{P}$  at  $\omega = 0$  constant for the two cases, the behavior under experimental conditions will of course depend on the actual amplitude of the low frequency noise.

We now turn to the perhaps more experimentally relevant situation of subsection 7.1, as represented by Fig 3. While the  $\mathbf{V}$  is still along the x-axis, the noise is now along the z-axis, (“flux noise” in the SQUID).  $\mathbf{P}$  is again started along the z-axis.

The noise perturbation along the z-axis leads to two differences with the x-noise case just discussed. One is that the shifts in the rotation frequency are now quadratic in  $B$ . One has  $V \rightarrow \sqrt{V^2 + B^2} \approx V + \frac{1}{2} \frac{B^2}{V}$ . Thus the magnitude of the alteration of  $\mathbf{V}$  is less than in the x-noise case, but will always have the same sign, leading to an increase of the average frequency of rotation, by  $\frac{1}{2V} \overline{B^2}$ . This average change is not relevant to the decoherence, but its fluctuations, characterized by  $\overline{B^4} - (\overline{B^2})^2$ , will play the role of the  $B$  fluctuations characterized by  $\overline{B^2}$  in the x-noise case.

The second difference has to do with the fact that since  $\mathbf{B}$  is no longer parallel to  $\mathbf{V}$ , the plane in which  $\mathbf{P}$  rotates is tilted somewhat with respect to the y-z plane. This will lead to some oscillatory effects in the projections of  $\mathbf{P}$ , but not to an increasing-with-time decoherence arising from the spread in rotation frequencies.

We thus again concentrate our attention on the spread in rotation frequencies. We repeat the arguments around Eq 32, with the role of  $B(t)$  now played by  $B^2(t)/2V$ . Eq 32 now becomes

$$\begin{aligned} \overline{P} &= \overline{\cos\left(\int_0^t \frac{B^2(t')}{2V} dt'\right)} \approx \overline{\cos\left(\frac{B^2}{2V}t\right)} = \int \cos\left(\frac{B^2}{2V}t\right) Prob(B) dB \quad (33) \\ &= \cos\left(\frac{1}{2} \arctan(\alpha t)\right) \frac{1}{(1 + \alpha^2 t^2)^{1/4}}, \end{aligned}$$

where we have taken a gaussian  $Prob(B)$  and  $\alpha = \overline{B^2}/V$ . For small  $t$  one has  $\overline{P} \approx 1 - (3/8)(\overline{B^2}/V)^2 t^2$ . As before,  $\overline{B^2}$  is the relevant parameter of the noise, but now it enters as  $(\overline{B^2})^2$  since we are now concerned with the fluctuations of  $B^2$  instead of those of  $B$ .

In Fig 10 we show z-noise simulations for  $\overline{P}$  with a low,  $\omega_c = 8 \times 10^{-5}$  and a higher  $\omega_c = 8 \times 10^{-4}$  frequency rectangular noise spectrum. The  $\delta\eta$  parameter of Eq 24 is  $2.5 \times 10^{-3}$ . One notes the above-mentioned oscillations. The envelope to the upper curve (dashed curve) can be fit with Eq 33 using  $\alpha = 5.3 \times 10^{-5}$ , while the prediction with the parameters used is  $\alpha = 6.4 \times 10^{-5}$ . Checks on the dependence of  $\alpha$  with respect to the magnitude and frequency of the noise signal are in agreement with the theory. The lower curve is fit by a simple exponential.

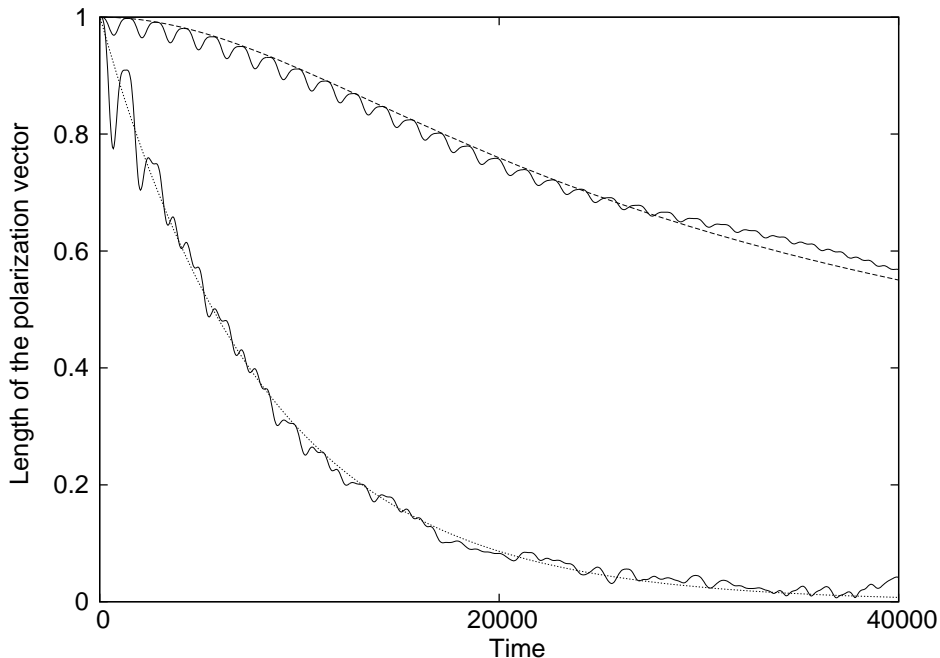


Figure 10: Simulations with a very low  $\omega_c = 8 \times 10^{-5}$ , and higher  $\omega_c = 8 \times 10^{-4}$ , frequency z-noise. The dashed line fitting the upper curve uses Eq33 with  $\alpha = 5.3 \times 10^{-5}$ . It exhibits the  $1 - \text{const}.t^2$  behavior at small times, with  $\text{const.} \sim (\overline{B^2})^2$ . The lower curve is fit with a simple exponential.

The fact that the decoherence here depends on  $\overline{B^2}$  or the integral over  $\mathcal{P}(\omega)$  leads to amusing consequences in the  $n=2,3$  “planckian noise” cases, where the  $\mathcal{P}(0)$  determining  $D$  is zero. As the temperature is lowered and  $\overline{B^2}$  becomes the relevant quantity, the decoherence could increase. We find this is indeed the case in simulations, with the decoherence increasing substantially for temperature  $\text{few} \times 10^{-3}$ , to above the  $D \sim 10^{-4}$  level.

A further interesting point to be noted is that in the general formalism the length of  $\mathbf{P}$  is always entropically decreasing (see Eq 17); while here, as in the oscillations in Fig 10,  $\mathbf{P}$  can in fact increase.

In general concerning very low frequency noise, we can conclude that there will be a spread of oscillation frequencies or “dephasing” at times  $t \ll t_{\text{noise}}$ , leading to a decoherence which is related to the variance of the noise signal  $\overline{B^2}$ , as opposed to the integral over the autocorrelation function determining  $D$ . It appears in different ways according to the type of noise, as in our examples of x- or z- noise. While with high frequency noise the  $t \ll t_{\text{noise}}$  regime may be unobservably small, with very low frequency noise it could dominate the relaxation of  $\mathbf{P}$ , as for the upper curve of Fig 9.

In this section we have retained the assumption of a small noise signal:  $B/V \ll 1$  and treated a constant  $V$ . In the low frequency limit for the noise



it would also be possible to treat a large  $B$ , and a slowly moving  $V$ , using the adiabatic approximation, but this is beyond the scope of the present discussion.

## 12 Conclusions

In summary, we have reviewed and extended the formulas relating random noise signals and the decoherence parameter for the effective two level system formed by the lowest levels of a double potential well. The random noise is applied as a fluctuation of various parts of the full multi-level hamiltonian. Numerical simulations verify the theoretical predictions, in which the relevant characteristic of the noise is the power at zero frequency. In particular different kinds of noise signals are applied and we find reasonable agreement between the simulations and the analytic predictions.

This agreement includes the size of the decoherence parameter, as well as its independence on the state of the system and on the frequency composition of the noise. Effects related to the excitation of levels beyond those constituting the two qubit-like states are discussed. The results confirm the possibility of describing the dynamics with an equation with a single decoherence constant  $D$ . “Collapse of the Wavefunction” behavior as well as that of the “Watched Pot Effect” are induced for large values of  $D$ . In general one finds that, within the allowable parameter ranges, the full complexity of the SU2 structure involving the noise vectors, the  $\mathbf{V}$  and the  $\mathbf{P}$  arises from the two-state reduction of the full hamiltonian. A particularly striking result, in agreement with the theory, is the small size or absence of decoherence when the noise signal has no power at zero frequency.

The noise power at zero frequency appears in fundamental treatments [16] [17] of the dissipation problem as the level of white noise. As is familiar from Johnson noise, for example, the existence of a classical dissipative parameter like resistance is associated with a constant noise spectrum at low frequency. We thus arrive at the perhaps obvious interpretation that to have a small  $D$  such classical dissipative effects or parameters should be kept to a minimum.

An interesting general question concerning our approach is to what extent classical random noise can be used as an adequate simulation of decoherence. A real, classical signal, that is an unquantized [18] field, causes as many transitions ‘up’ as ‘down’ between any pair of states. This means that “spontaneous emission” or “relaxation”, where, even in the absence of any noise, an upper level emits a quantum (e.g. a phonon, or in vacuum a photon) and transits to the lower state is absent. On the other hand, the neglect of spontaneous emission may not be important in practice. Quantum logic devices should have short time scales of operation, while spontaneous emission rates will be slow. Study of this question would require a detailed analysis for specific devices.

While our main results are in the context of standard high frequency noise, we also offer a short discussion and simulations of noise signals dominated by low frequencies. It is found and verified by the simulations that in this case the relevant parameter becomes the variance or integral over the power spectrum

of the noise.

## 13 Acknowledgements

We would like to acknowledge the participation of A. Görlich in the development of the software set.

This work was partially supported by the International PhD Projects Programme of the Foundation for Polish Science within the European Regional Development Fund of the European Union, agreement no. MPD/2009/6.

## References

- [1] V. Corato, P. Silvestrini, A. Görlich, P. Korcyl, L. Stodolsky, and J. Wosiek, Phys. Rev. **B75** 184507 (2007); arXiv:cond-mat/0611445.
- [2] For more on the physical units for the SQUID and their translation into other terms see the section “Squid Hamiltonian” of [1].
- [3] J. Wosiek, *Nucl. Phys.* **B644** 85 (2002); hep-th/0203116.
- [4] See the discussion “Hilbert space completeness” in [1].
- [5] In order that the  $\mathbf{B}$  appear as small changes in the  $\mathbf{V}$ , we have included a factor of  $\frac{1}{2}$  in the definition of the random field hamiltonian which was not present in [1]. This different normalization of the  $\mathbf{B}$  accounts for the factor 4 difference between Eq 16 here and the equivalent Eq 23 of [1].
- [6] Alternatively, one may use  $\lambda\mathbf{B}$  instead of  $\mathbf{B}$  to keep track of the orders in  $\mathbf{B}$  and then set  $\lambda = 1$  at the end.
- [7] See Eq 16 of [1].
- [8] L. Stodolsky and P. Silvestrini, Physics Letters **A280** 17-22 (2001), arxiv:cond-mat/0004472.
- [9] I. B. Khriplovich and V. V. Sokolov, *Physica* **A**, 73, (1987).
- [10] See for example the relation connecting the diffusion constant and the velocity autocorrelation function on page 251 of *Introduction to Modern Statistical Mechanics*, by David Chandler, Oxford University Press, 1987.
- [11] R. A. Harris and R. Silbey, *J. Chem Phys.* **78** 7330 (1983).
- [12] One might be tempted to try to evaluate the  $x^2$  factor in Eq 28 by using our association  $x \approx x_c \sigma_z$ . This would evidently be wrong, since it leads to no change in the energy splittings. The reason for this is that the evaluation of the matrix elements of the  $x^2$  operator goes beyond the two-state model, and involves the whole Hilbert space of the  $x$  variable. Our problem

provides a nice example of how in an effective theory –here the two-state hamiltonian Eq 2 – one obtains a simplification at the price of some unknown parameters, (e.g. matrix elements of  $x^2$ ) which are only determined in the more complete theory–here the full hamiltonian Eq 1.

- [13] For recent discussions of dominant low frequency noise for SQUIDs see M. H. S. Amin and D. V. Averin, *Phys. Rev. Lett.* **100** 197001 (2008) and R. Harris, M. W. Johnson, et al. *Phys. Rev. Lett.* **101** 117003 (2008). It should be noted that the transition rate formulas in these papers are those of the “Turing” or “Watched Pot ” effect. That is, the rate is given by the tunneling energy squared divided by the noise/decoherence parameter, as in our Eq 29. As explained in Ref [14] this arises as simply the solution of our Eq 5 for large  $D$ :  $P_z \approx 1 - (\omega_{tunnel}^2/D)t$ . Since  $\omega_{tunnel}$  in Harris, Johnson, et al. appears to be quite small the stabilization of the state could be very strong. ( For simulations see Fig 6 of Ref [1]. ) Then sub-dominant effects, not necessarily related to the tunneling interaction, could induce transitions. Thus an alternative explanation of the data of Harris, Johnson et al. might be possible where the “Watched Pot Effect” keeps the system in the upper state long enough that a slow “spontaneous emission” to the ground state can be observed. A test of this interpretation could be carried out by performing the procedure of Ref [8], namely a determination of  $D$  by means of an adiabatic sweep of  $x^{ext}$  through the “resonance” or “level crossing”.
- [14] R.A. Harris and L. Stodolsky, *Phys. Lett.* **B116** 464 (1982). For a general introduction and review of these concepts see L. Stodolsky, “Quantum Damping and Its Paradoxes” in *Quantum Coherence*, J. S. Anandan ed. World Scientific, Singapore (1990).
- [15] L.Stodolsky “Coherence and the Clock”, section X, in *Time and Matter* I. Bigi and M. Faessler, eds., World Scientific, (2006); quant-ph/0303024 . The positivity of the  $DP_T$  terms corresponds to the positivity of a certain tensor in the general case, see ref [9].
- [16] G. W. Ford and M. Kac, *Jnl. Stat. Phys.* **46** 803 (1987). We note that in view of our observation of the importance of the spatial dimension through its effect on the noise power at  $\omega = 0$ , the assumption of working in one dimension in this reference may not be entirely innocent.
- [17] A. O. Caldeira and A. J. Leggett, *Physica* **121 A** 587 (1983).
- [18] See the discussion in R.P. Feynman and A. R. Hibbs, *Quantum Mechanics and Path Integrals*, McGraw-Hill (1965), around Eq 12-113 concerning the reality of the  $\alpha$  parameter in the influence functional formalism.